Proceedings of the International Conference
on Solid-Solid Phase Transformations '99 (JIMIC-3)
Edited by M. Koiwa, K. Otsuka and T. Miyazaki
The Japan Institute of Metals, 1999.

Computer Simulation of Atomic Lattice Models for Phase Separation in Alloys with Coherent Lattice Misfit

Peter Fratzl[1], Oliver Penrose[2] and Joel L. Lebowitz[3]

[1] Erich Schmid Institute of Materials Science, Austrian Academy of Sciences,
and University of Leoben, Jahnstr. 12, A-8700 Leoben, Austria
[2] Department of Mathematics, Heriot-Watt University,
Riccarton, Edinburgh EH14 4AS, Scotland, UK
[3] Departments of Mathematics and Physics, Rutgers University,
Hill Center, Busch Campus, New Brunswick, 08903 New Jersey, USA.

Keywords: Monte-Carlo simulation, phase separation, decomposition, coherent precipitates, misfit, coarsening, directional growth, rafting.

Abstract

We use computer simulations on the atomic level to study phase separation in binary alloys with elastic misfit. The model considers a lattice of A and B atoms of different size connected by harmonic forces that need not necessarily be central. The atomic positions may deviate from the lattice sites due to internal strains induced by the elastic misfit. Diffusion is modeled by exchanges of A and B atoms and simulations of the morphological evolution during phase separation are performed using Monte Carlo techniques. Results were obtained for two-dimensional square lattices with cubic elastic anisotropy. We have studied the coarsening of anisotropic domains, the effects of an ordering tendency in the precipitates and the influence of externally applied stress ("rafting").

Introduction

A large number of computer simulations of the phase separation process under the influence of elastic misfit strains have appeared in recent years. These were based either on macroscopic models where precipitates are considered to be separated by sharp interfaces and the misfit interactions are treated by continuum elasticity [1-4], or on mesoscopic models based on modified Cahn-Hilliard equations [5-12], or finally on atomistic simulations where the elastic interactions are represented by springs connecting the atoms [13-16]. A detailed discussion of these approaches has been given in a recent review of the subject [17].

Fig. 1 shows typical morphologies in phase separating alloys without (a,b) and with positive (c,d) or negative (e,f) lattice misfit between precipitates and matrix. One of the main features arising from elastic misfit interactions with cubic anisotropy is a clear breaking of the spherical symmetry. Externally applied stress leads to a further symmetry breaking and to the development of a parallel-plate morphology (g,h). These properties have to be reproduced by any attempt to model such alloys.

In this paper, we summarize results on the morphological evolution of binary alloys which we have obtained using atomistic simulations [14-16].

The model

Our model [14] for a crystalline solid is a lattice (with periodic boundary conditions) where each of the N sites is occupied by either an A or a B atom. We define a "spin" function $\gamma(\mathbf{p})$ by $\gamma(\mathbf{p}) = 1$ if there is an A-atom at site $\mathbf{p}$ and $\gamma(\mathbf{p}) = -1$ if there is a B-atom

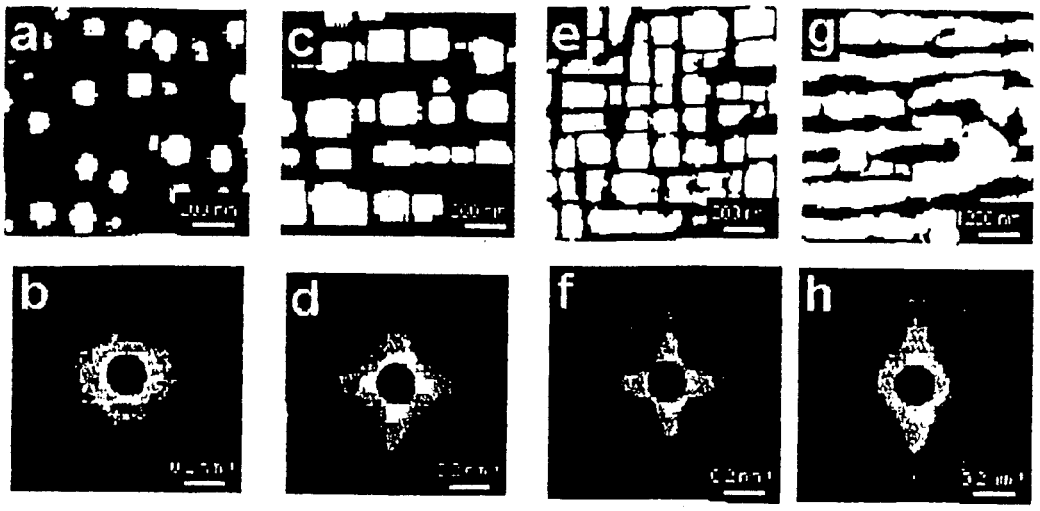

Fig. 1: (a) Transmission electron micrograph (TEM) of Ni-Al-Mo alloy with Mo-concentration chosen such as to make the lattice spacing in matrix and precipitates (gamma-prime phase) equal. Treatment: 430h at 1048 K after quench from the single-phase region. The plane of observation corresponds to the crystallographic plane (001). One observes round precipitates *i.e.* no elastic effects.
(b) Small-angle X-ray scattering (SAXS) data from the same specimen in the same orientation. One observes an isotropic scattering pattern, that is, spherical symmetry in both the shape and the distribution of precipitates.
(c) TEM of the (001)-plane of a Ni-Al-Mo alloy with Mo-composition chosen such as to make the lattice spacing in the precipitates (gamma-prime phase) larger by 0.4%. Same thermal treatment as in (a). One observes cube-like precipitates, aligned along the elastically soft directions, [010] and [100].
(d) SAXS from the specimen in (c). There is a flower-like pattern with four-fold symmetry, the elongations being in [010] and [100]-directions (indicating flat interfaces and strong correlations in those directions). This picture clearly shows that the spherical symmetry was broken and that cubic symmetry appeared in the shape and in the arrangement of the precipitates.
(e) TEM of Ni-Al-Mo alloy with Mo-composition chosen such as to make the lattice spacing in the precipitates (gamma-prime phase) smaller (misfit -0.5%). Treatment: 5h at 1253K (Orientation 001). Patterns qualitatively similar to those in (c).
(f) SAXS from the specimen in (e). Qualitatively, the patterns are similar to the case with positive elastic misfit (c,d).
(g) Same alloy and heat-treatment as in (e), but now with a external compressive load of 130MPa applied to it along the vertical [010]-direction.
(h) SAXS from the specimen in (g). Note that the horizontal streak has disappeared, corresponding to the disappearance of vertically oriented interfaces in (g). This corresponds to a further symmetry breaking towards a tetragonal symmetry in the shape and arrangement of precipitates.
The data in (a)-(d) are taken from [19] and in (e)-(h) from [18].

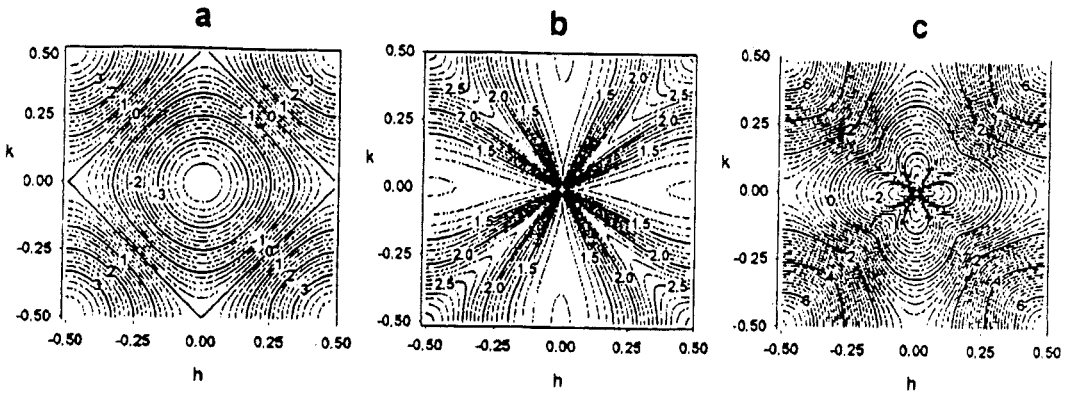

Fig. 2: Contour plot of typical interaction potentials in the first Brillouin zone of a square lattice. (a) Short-range potential $C(\mathbf{k})$ due to attractive nearest neighbor chemical interaction between like neighbors. This potential is isotropic near the origin of k-space. (b) Elastic potential $E(\mathbf{k})$ for negative cubic anisotropy considering harmonic interactions to the first and second nearest neighbors. This potential has a discontinuity at the origin of k-space and is strongly orientation dependent, with minima in (10) and (01) directions. (c) Total potential $\Psi(\mathbf{k})$ given as the sum of $C(\mathbf{k})$ and $E(\mathbf{k})$ (see Eq. 1). This potential has a minimum near the origin of k-space but has cubic anisotropy with lower values in the (10) and (01) directions than in others (from [14]).

at this site. The atoms are assumed to interact "chemically" over short distances, with like atoms attracting one another. If the atoms are of different sizes, elastic interactions will be important. The interatomic forces are modeled by assuming that pairs of atoms are joined by linear springs. In the simplest case, considered here, the stiffness of these springs does not depend on the type of atom they are connecting. This means that the elastic properties of the crystal are assumed independent of composition. The lengths of the springs, however, depend on the deviation of the atoms from their equilibrium positions, as well as on the sizes of the atoms on both ends of the spring.

For any given arrangement of A and B atoms over the N lattice sites, it is assumed that the atoms relax rapidly into the positions near their assigned lattice sites that minimize the elastic energy, so that the energy depends only on the arrangement of atoms, that is on the function $\gamma(\mathbf{p})$. The total energy of the system can then be written as ([14] and references therein)

$$E = \frac{1}{2N} \sum_{\mathbf{k}} \Psi(\mathbf{k}) \, |\Gamma(\mathbf{k})|^2 + \text{constant}, \tag{1}$$

where the sum extends over the first Brillouin zone of the lattice and where we define

$$\Gamma(\mathbf{k}) = \sum_{\mathbf{p}} \gamma(\mathbf{p}) e^{i\mathbf{p}\cdot\mathbf{k}} \tag{2}$$

The total potential $\Psi(\mathbf{k})$ is the sum of two terms, $E(\mathbf{k})$, due to the internal strains, and $C(\mathbf{k})$ representing the short-range chemical interaction between the atoms. Fig. 2 shows a plot of all three potentials, $\Psi(\mathbf{k})$, $E(\mathbf{k})$ and $C(\mathbf{k})$ for a typical situation in a planar square lattice with cubic anisotropy.

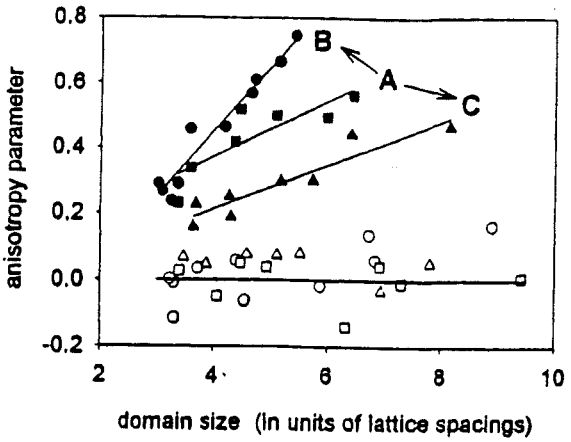

Fig. 3: Cubic anisotropy parameter α (Eq. 5) as a function of the typical domain size during coarsening. (A) corresponds to phase separation with a concentration $c = 0.5$ of B atoms and a temperature $T/T_c = 0.8$, T_c being the critical temperature. The anisotropy grows faster when the temperature is smaller at fixed composition (B, corresponding to $T/T_c = 0.4$ and $c = 0.5$) and grows more slowly if the concentration is decreased at constant temperature (C, corresponding to $c = 0.2$ and $T/T_c = 0.8$). These simulations (full symbols) were carried out using the potential shown in Fig. 2c. For comparison, simulations were also performed with the same short-range potential but no elastic misfit using the potential shown in Fig. 2a. Without misfit, the anisotropy parameter fluctuates around its zero value (open symbols) [14].

Coarsening of misfitting precipitates

Computer simulations were carried out for a square lattice using the potential $\Psi(\mathbf{k})$ shown in Fig. 2c [14]. It was found that the domain patterns become increasingly anisotropic corresponding to a progressive alignment along lines and columns. For a quantitative analysis of the time dependence of the anisotropy, we use the structure function

$$I(\mathbf{k}) = |\sum_{\mathbf{p}} \gamma(\mathbf{p})\, e^{i\mathbf{k}\cdot\mathbf{p}}|^2 = |\Gamma(\mathbf{k})|^2 \tag{3}$$

and $I(\mathbf{k}) = I(k,\theta)$, where the zero of the polar angle θ is taken along a (10)-direction of the lattice, to define:

$$J_n = \int_{(2n-1)\pi/8}^{(2n+1)\pi/8} d\theta \int_0^{\pi/a} dk\; I(k,\theta) \qquad (n = 0,\ldots,7) \tag{4}$$

As a measure of the anisotropy we use a parameter α which characterizes the deviation from radial symmetry:

$$\alpha = \sum_{p=0}^{3} (J_{2p} - J_{2p+1}) \;/\; \sum_{n=0}^{7} J_n \tag{5}$$

Fig. 3 gives the evolution of α as a function of the typical domain size R, defined as the first zero of the two-point correlation function, that is, the Fourier transform of $I(\mathbf{k})$. Fig. 3 clearly shows that - for a given size of the domains - the morphology is less isotropic for coarsening at lower temperatures or at higher volume fraction. The anisotropy parameter

computed for comparison using a potential without elastic misfit (Fig. 2a) did not deviate significantly from zero (open symbols in Fig. 3).

When analyzing the time-dependence of the domain size, we obtained the surprising result that all data (regardless of whether elastic misfit was considered or not) could be described to a good approximation by the function

$$R = R_0 + a\,(t/t_0)^{\beta} \qquad \text{with} \qquad \beta = 1/3 \tag{6}$$

where t is the time, t_0 and R_0 are constants and a is the lattice constant of the square lattice. The constant R_0/a was between two and three at all temperatures and concentrations investigated, both with and without elastic misfit. Only the constant t_0 showed a clear increase with increasing lattice misfit [14]. This indicates some slowing down of the coarsening kinetics due to the misfit interaction but no change in the growth exponent β.

Externally applied stress

When external stress is applied to an alloy with misfitting precipitates, the coarsening process may be considerably changed by the occurrence of directional coarsening or "rafting" [3,4,18]. The reason is a coupling of the external strain to the composition field in the specimen which requires composition dependent elastic constants. But such a composition dependence was excluded by the assumptions in the model discussed in the previous section. The model can, however, be extended by assuming that the stiffness of each spring depends weakly on the type of atoms it is connecting [15], simply by writing for a typical stiffness L:

$$L(\mathbf{p}) = L_0 + \delta\,[\gamma(\mathbf{p}) + \gamma(\mathbf{p}')]/2 \tag{7}$$

where $\mathbf{p}'$ is the position of the neighbor connected to $\mathbf{p}$ by the spring. L_0 and δ are constants and $\delta << 1$. The difficulty arising from this assumption (eq. 7) is that non-linear terms appear in the equations for elastic equilibrium. A rough approximation can be obtained, however, by a linearization of those equations [15]. The total energy can then again be expressed by an equation similar to Eq.(1), with a k-space potential $\Psi(\mathbf{k})$ that depends on δ and the external stress. If the external stress is uniaxial, the potential has a tetragonal instead of the quadratic symmetry seen in Fig. 2c. The consequence is that the precipitate arrangement evolves towards a series of stripes with "wavy" character, very much like those seen in some experiments (Fig.1g), which are either parallel of perpendicular to the stress direction, depending on the sign of δ and of the external stress [15].

Despite this considerable change in morphology due to the external stress, the thickness of the stripes was shown in simulations to be growing according to Eq.(6). Only the length of the stripes is increasing at a much faster rate. In this two-dimensional model, there is no essential difference between compressive or tensile uniaxial load, except that the direction of the stripes is parallel to the load direction in one case and perpendicular to it in the other. This is a clear defect of the 2-D model, because in three dimensions one would expect the precipitates to be plates if they are perpendicular to it, or rods if parallel to it. There is, of course, no reason why the coarsening kinetics of parallel plates should be the same as for parallel cylinders, while in two dimensions both situations reduce to the same morphology, namely stripes.

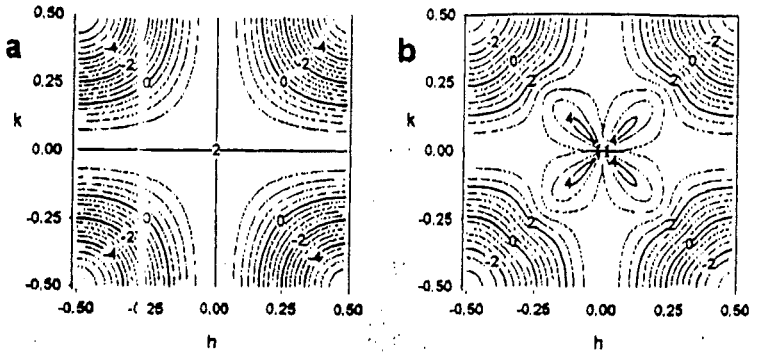

Fig. 4: (a) Short-range potential $C(\mathbf{k})$ for the model with repulsive nearest neighbor and attractive next-nearest neighbor interaction of like atoms. (b) Total potential $\Psi(\mathbf{k})$, computed as the sum of the potentials in Figs. 4a and 2b.

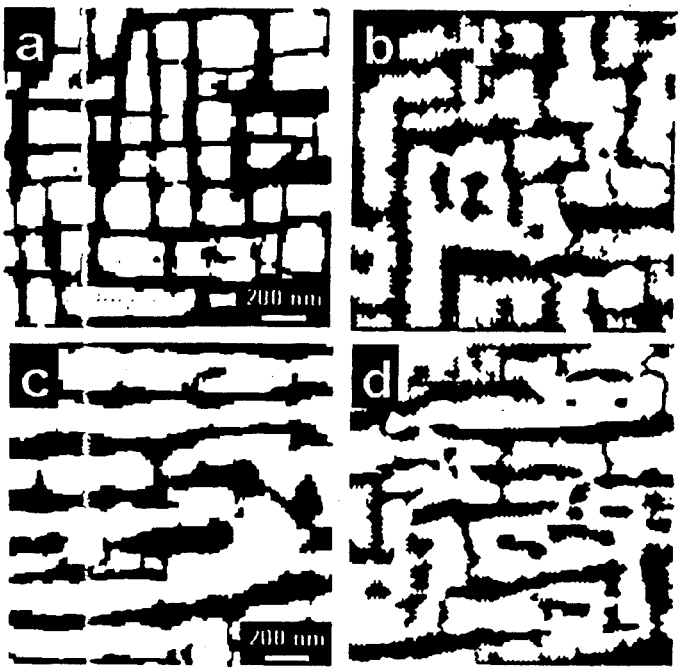

Fig. 5: (a) and (c) are reproductions of Figs1(e) and 1(g), respectively. (b) shows results from computer simulations with repulsive interaction of like atoms on nearest neighbor sites and attractive interaction of like atoms on next nearest neighbor sites (using the potential $\Psi(\mathbf{k})$ shown in Fig. 4b). Black shows the disordered phase (containing mostly A-atoms) and white the ordered phase (consisting of about half A and half B atoms). The overall concentration of B-atoms was 0.35. (d) The same model, temperature and annealing time as in (b), but with an additional external load along the vertical direction (simulations from [16])

Precipitates with interatomic order

The most extensively investigated alloy system where elastic misfit interactions play an important role comprises the nickel-base superalloys. Many typical features, like the appearance of the cubic symmetry due to the misfit interactions as well as the rafting phenomenon, are reasonably well described in the atomistic model discussed in the foregoing. An important property that was neglected in this approach is the fact that the precipitates in nickel-base superalloys correspond to an ordered intermetallic phase.

To investigate the influence of atomic ordering within our atomistic model, we may change $C(\mathbf{k})$ keeping $E(\mathbf{k})$ the same: Instead of an attractive interaction between like atoms, we now use a repulsive interaction (energy J) between like atoms on nearest neighbor sites and on attractive interaction (energy $J/2$) between next-nearest neighbors. The resulting potentials for Eq.(1) are shown in Fig. 4. Both, $C(\mathbf{k})$ and $\Psi(\mathbf{k})$, are now minimal at the reciprocal lattice point $(\frac{1}{2},\frac{1}{2})$, which means that the solid solution at high temperatures has the primary tendency to undergo ordering. Phase separation is only a secondary effect due to the existence of a triple point below which a miscibility gap exists. Since the potential $\Psi(\mathbf{k})$ has a discontinuity close to the origin with larger values along the diagonals (Fig. 4b), an alignment of the precipitates along the horizontal and vertical directions will be preferred during phase separation within this miscibility gap.

Most of the conclusions about coarsening and rafting stay the same in this modified model [16]. The major difference arises from the fact that there exist several variants for the ordered phase, according to which sublattice is occupied by A atoms or by B atoms. In the simple model on the square lattice there are two such variants, for other lattices or in three dimensions there could be more. When the ordered phase is the minority phase, the model leads - as expected - to the formation of ordered precipitates in a disordered matrix. When the ordered phase is the majority phase, however, the situation is quite different. By analogy one would expect precipitates of the disordered phase in a matrix of ordered phase. Since not all of the ordered phase will have nucleated as the same variant, such a domain morphology would lead to anti-phase boundaries (APB) between the variants. These APB's have a larger energy in our model than the boundaries between ordered and disordered phase. Hence, they will be wetted by the disordered phase. The result is that the disordered minority phase wraps precipitates of ordered phase, an effect also found by other approaches [8,10]. Given the smaller volume fraction of the disordered phase, the channels between ordered precipitates can be quite narrow. Such a situation is shown in Fig. 5 which also includes the case of rafting under external load. The similarity in these pictures between simulations and experiment is quite striking.

Conclusions

Using a conceptually very simple atomistic model and performing computer simulations in two dimensions, many details about phase separation in alloys with misfitting precipitates can be reproduced correctly. This includes the appearance of cubic anisotropy in the precipitate morphology as well as coarsening kinetics. Even the typical effects of externally applied stress can be reproduced. There are, however, also a number of difficulties with such simulations:

First, only small specimen sizes can be modeled by such an approach. Since the effect of the elastic misfit increases with precipitate size, unrealistically large misfits have to be assumed in the atomistic model, in order for the effects of the misfit to appear at the small precipitate sizes accessible to computer simulation.

Second, some important aspects may be missed by the two-dimensional character of the

simulations. An example is the difference between compressive and tensile load in the case of rafting. While one expects either plates perpendicular to the stress direction or cylinders parallel to it, depending on the direction of the load, both situations reduce to stripes in the two-dimensional case. This is, however, not a fundamental problem and first results have already been obtained with a three-dimensional model [20].

Third, the Fourier method which gives Eq. (1) is based on the assumption that the stiffness of the springs does not depend on the type of atoms it connects. This means that the elastic constants are assumed independent of composition which is quite unrealistic in some cases. To avoid this, it appears necessary to treat configuration variables $\gamma(\mathbf{p})$ and strain variables independently [13].

As a whole, the atomistic simulations show that many of the effects due to misfitting precipitates can be understood by simple interatomic interactions. They are also useful in the description of precipitation at very small scale. For the simulation of larger scale structures, it may be more appropriate, however, to approach the problem by other methods such as the diffuse interface model [5-12].

References

1) P. W. Voorhees, G. B. McFadden and W. C. Johnson: Acta Metall. Mater. **40** (1992), 2979-2992.
2) T. A. Abinandanan and W. C. Johnson: Acta Metall. Mater. **41** (1993), 17-25; ibidem, 27-39.
3) W. Hort and W. C. Johnson: Met. and Mater. Trans. **27A** (1996), 1461-1476.
4) C. H. Su and P. W. Voorhees: Acta Mater. **44** (1996), 1987-2000; ibidem, 2001-2016.
5) H. Nishimori and A. Onuki: Phys. Rev. B **42** (1990), 980-983.
6) A. Onuki and H. Nishimori: Phys. Rev. B **43** (1991), 13649-13652.
7) Y. Wang, L.-Q. Chen and A. G. Khachaturyan: Acta Metall. Mater. **41** (1993), 279-296
8) C. Sagui, A. M. Somoza and R. Desai: Phys. Rev. E **50** (1994), 4865-4879.
9) Y. Wang and A. G. Khachaturyan: Acta Metall. Mater. **43** (1995), 1837-1857.
10) Y. Wang and A. Khachaturyan: Phil. Mag. A **72** (1995), 1161-1171.
11) T. Koyama, T. Miyazaki and A. E. Mebed: Metal Mater. Trans. A **26** (1995), 2617-2623.
12) Leo P. H., J. S. Lowengrub and H. J. Jou: Acta Mater. **46** (1998), 2113-3130.
13) J. K. Lee: Mater. Sci and Eng. **A 238** (1997), 1-12; Mater. Trans. JIM **39** (1998), 114-132.
14) Fratzl P. and O. Penrose: Acta Metall. Mater. **43** (1995), 2921-2930; ibidem **44** (1996), 3227-3239.
15) C. A. Laberge, P. Fratzl and J. L. Lebowitz: Phys. Rev. Lett. **75** (1995), 4448-4451; Acta Mater. **45** (1997), 3949-3961.
16) P. Nielaba, P. Fratzl and J. L. Lebowitz: J. Stat. Phys. (in press, 1999).
17) P. Fratzl, O. Penrose and J. L. Lebowitz: J. Stat. Phys. (in press, 1999).
18) O. Paris, M. Fährmann, E. Fährmann, T.M. Pollock and P. Fratzl: Acta Mater. **45** (1997), 1085-1097.
19) M. Fährmann, P. Fratzl, O. Paris, E. Fährmann and W. C. Johnson: Acta Metall. Mater. **43** (1995), 1007-1022.
20) H. Gupta, R. Weinkamer, P. Fratzl and J. L. Lebowitz: These proceedings.